bioRxiv preprint doi: https://doi.org/10.1101/658831; this version posted June 3, 2019. The copyright holder for this preprint (which was not certified by peer review) is the author/funder, who has granted bioRxiv a license to display the preprint in perpetuity. It is made available under aCC-BY 4.0 International license.

3D-printed moulds of renal tumours for image-guided tissue sampling in the clinical setting

Mireia Crispin-Ortuzar[1*,◕], Marcel Gehrung[1◕], Stephan Ursprung[1,2], Andrew B Gill[2], Anne Y Warren[3], Ferdia A Gallagher[2], Thomas J Mitchell[4,5], Iosif A Mendichovszky[6] Andrew N Priest[6,2], Grant D Stewart[4‡], Evis Sala[1,2‡], Florian Markowetz[1*‡]

1 Cancer Research UK, Cambridge Institute, University of Cambridge, UK
2 Department of Radiology, University of Cambridge, UK
3 Department of Histopathology, Cambridge University Hospitals NHS Foundation Trust, Cambridge, UK
4 Department of Surgery, University of Cambridge, UK
5 Wellcome Trust Sanger Institute, Hinxton, CB10 1SA, UK
6 Department of Radiology, Cambridge University Hospitals NHS Foundation Trust, Cambridge, UK

◕These authors contributed equally to this work.
‡Shared senior authorship.
* mireia.crispinortuzar@cruk.cam.ac.uk, florian.markowetz@cruk.cam.ac.uk

Abstract

Spatial intratumoural heterogeneity is a major challenge in precision medicine. Progress to better understand the relationship between genetic heterogeneity and tissue heterogeneity depends on accurately co-registering imaging data and tissue samples. We address this challenge in patients with renal cell carcinoma undergoing radical nephrectomy and propose a computational approach to produce patient-specific 3D-printed moulds that can be used in the clinical setting. Our approach achieves accurate co-registration of sampling location between tissue and imaging, and integrates seamlessly with the clinical, imaging and pathology workflows. It also provides image guidance for tissue sampling while respecting pathologists' preference for specific cutting planes, irrespective of the presence of perinephric fat. The methodology is tested on a patient undergoing radical nephrectomy, obtaining Dice similarity coefficients between imaging and tissue ranging from 0.75 to 0.92. Our work provides a robust and automated interface between imaging and tissue samples, enabling the development of clinical studies to dissect tumour heterogeneity at multiple scales.

Author summary

Cancer is a complex disease. Different parts of a single tumour often look different in medical images; they sometimes even carry different genetic information. This complexity may be key to understanding why some tumours respond better to therapy than others. Once the tumour has been removed through surgery, we can obtain tissue samples that allow us to study its spatial composition. However, matching these data to the images that were obtained before surgery is challenging. We have developed a computational methodology that relies on 3D printing to create tumour moulds that help us match images and tissue accurately. In addition, unlike previous approaches, our technology does not disrupt clinical practice, so it can be used routinely.

bioRxiv preprint doi: https://doi.org/10.1101/658831; this version posted June 3, 2019. The copyright holder for this preprint (which was not certified by peer review) is the author/funder, who has granted bioRxiv a license to display the preprint in perpetuity. It is made available under aCC-BY 4.0 International license.

Introduction

Molecular tumour profiling is used to stratify patients and identify new actionable targets for precision therapeutics. The assessment is typically based on data from a single tumour biopsy [1]. Often, however, tumours display such a high degree of heterogeneity that a single tissue sample is insufficient to capture the full molecular landscape of the disease [2]. A prime example of such spatial heterogeneity is renal cell carcinoma (RCC), which has been shown to be radiologically, genetically, and metabolically heterogeneous [3–5]. Macroscopic regions with distinct genotypes can be identified within a single tumour through multiregional sampling [3, 6]. In parallel, radiological imaging provides non-invasive, three-dimensional information on phenotypic heterogeneity [7, 8]. The fact that RCC displays spatial heterogeneity at such disparate physical scales suggests that a combined approach to integrate the relevant data sources (genomics, transcriptomics, radiomics) is needed to unravel the complexity of the disease [9]. This would provide the necessary tissue context and macroscopic dimension to studies of genomic tumour evolution [4, 10–12]. The foundation of a combined analysis is the accurate spatial co-registration of imaging data and biopsies. However, accurate multiregional tumour biopsies can only be obtained after nephrectomy, when image-guidance is no longer a possibility.

The challenge of co-registering *in vivo* images to resected tumours has been addressed in other contexts. Previous solutions included holding the specimen with a cradle [13] or solidified agar [14]. However, these approaches had several disadvantages, including not being clinically usable, or not providing accurate orientation. More recently, personalised 3D moulds have been used to improve the accuracy of co-registration in prostate cancer [15–17] and ovarian cancer studies [18].

In RCC, however, 3D-printed moulds remain comparatively underexplored [19], as it presents unique challenges. The first challenge arises from the pathology guidelines for assessment of radical nephrectomy specimens, which requires optimal visualisation of the renal sinus–tumour interface. The most commonly adopted initial plane of incision is along the long axis at midpoint, with further sectioning usually perpendicular to this plane [20–22]. Thus, the sectioning planes are in general not the same as those used for imaging. An additional challenge is that pathologists need to preserve the integrity of some structures which are required for staging, such as the renal vein. Finally, the specimen is often covered by a thick layer of perinephric fat [23], which further complicates the procedure and can make it impossible to identify relevant structures.

Because of these restrictions, previous 3D-printing-based co-registration methods for RCC have either been limited to pre-clinical models [24], or have only focused on early-stage partial nephrectomy cases [25], where the fat-free resection margin can be used as a base for sectioning. In addition, none of them addressed the issue of having different sectioning and imaging planes. New methods are therefore needed to accurately match macroscopic habitats defined by imaging to specific tissue regions. Importantly, these methods need to integrate smoothly into the clinical pathway to allow future use in clinical trials and potentially clinical practice.

Here we report the design and implementation of a method to obtain multiple tissue samples accurately registered to a pre-surgical multiparametric magnetic resonance imaging (MRI) in patients undergoing radical nephrectomy for suspected RCC. Our methodology is based on a patient-specific 3D printed mould and is tailored for seamless integration with the clinical workflow:

1. Our approach respects the orientation of sectioning required for pathology examination;

2. Our approach transforms MRI images onto the pathology sectioning space, and provides slice-wise image-based tumour habitat maps that guide tissue sampling;

bioRxiv preprint doi: https://doi.org/10.1101/658831; this version posted June 3, 2019. The copyright holder for this preprint (which was not certified by peer review) is the author/funder, who has granted bioRxiv a license to display the preprint in perpetuity. It is made available under aCC-BY 4.0 International license.

3. Our approach uses a landmark-based method that enables orientation of specimens obscured by a large adipose layer.

These features make our method a substantial step forward towards creating datasets with accurately matched imaging, histological and genomics data. Below we present the computational details of the method, provide an in-depth protocol on how it can be generally applied to solid human tumours, and use a RCC radical nephrectomy case as an example.

Results

The mould is a three-dimensional block, with vertical slits that guide the sectioning, and a cavity designed to precisely fit the resected specimen, as shown in Figure 1. The shape of the cavity is derived from the 3D volumes drawn by a radiologist on a MR image of the tumour, which are rotated until the tumour is oriented along the desired direction inside the mould.

Our method therefore has four steps: (1) image segmentation, (2) image re-orientation and clustering, (3) mould optimisation and 3D printing, and (4) habitat sampling (Figure 1). This report focusses on the first three steps to design patient specific moulds. The method was designed to be as robust, reproducible and automated as possible. Steps (2) and (3) are fully automated. Step (1) requires manual intervention, but is assisted by computational techniques. This set-up aims to minimize experimental errors and facilitates the adoption of the method by other research groups. Figure 2 illustrates how these steps are integrated into the clinical workflow.

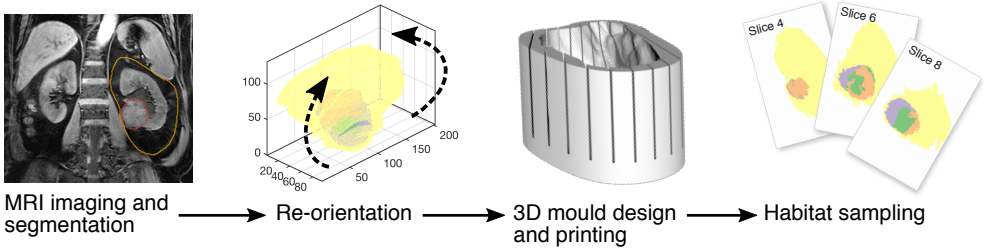

Fig 1. Overview of our approach The schematic depicts the four steps of the method bridging from MRI scans to spatial surgical biopsies. The method starts with the delineation of a MRI scan, which is then re-oriented, carved into a 3D-printed mould, and used for spatially accurate surgical biopsies. The slots of the mould guide the knife for cutting.

Personalised 3D mould design

Step 1: Image segmentation

Our approach requires two types of regions of interest (ROIs) to be drawn on the images: tissue segmentations and anatomic landmarks. Tissue segmentations are needed to test the spatial accuracy of the framework; they include the tumour, normal kidney, renal pelvis, and perinephric fat. Combined, they form the global outline of the specimen, which defines the shape of the mould. The centroid of the outline volume is referred to as the *absolute* centroid (C_0).

In addition, four anatomic landmarks are needed to determine the correct orientation of the specimen inside the mould. The first two are the upper and lower poles of the kidney, which are needed to ensure that the kidney can be sectioned along

bioRxiv preprint doi: https://doi.org/10.1101/658831; this version posted June 3, 2019. The copyright holder for this preprint (which was not certified by peer review) is the author/funder, who has granted bioRxiv a license to display the preprint in perpetuity. It is made available under aCC-BY 4.0 International license.

its long axis at midpoint [20]. The other two anatomic landmarks are the hilum and the area of the tumour with the thinnest fat coverage, referred to as the 'tumour contact' point. They are used to ensure that the specimen is accurately positioned.

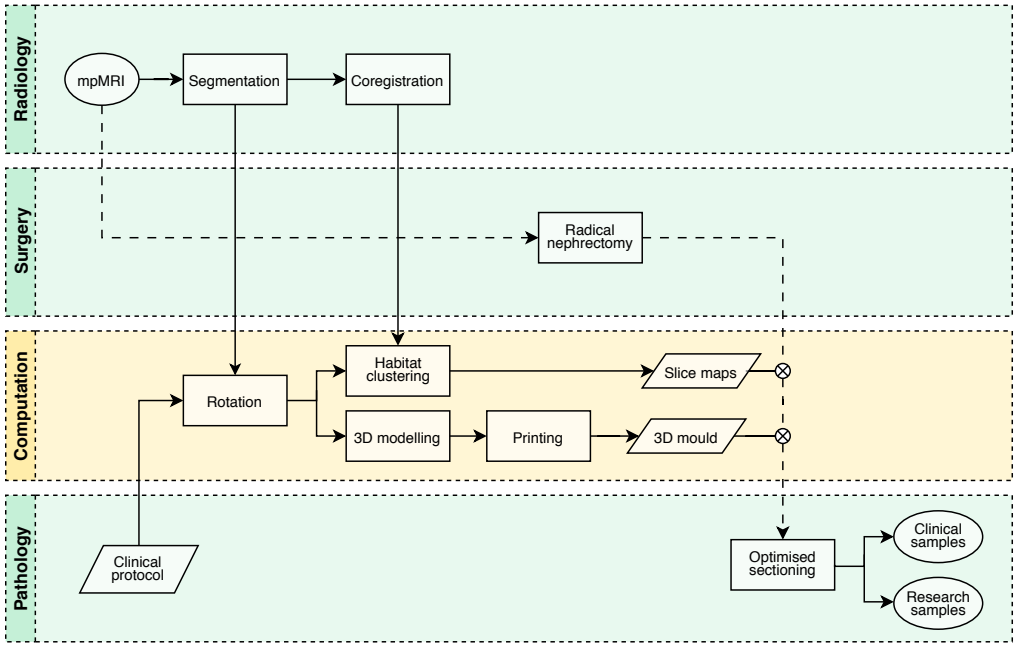

Fig 2. Integration of the clinical and computational pipelines. Flow chart of the different analysis steps performed by the radiology, surgery, pathology and computational groups to ensure seamless integration between the clinical and research arms. The yellow box highlights the computational steps of the pipeline.

Step 2: Image orientation

Our approach is designed to address the two key challenges explained in the introduction, both of which can be solved by controlling the orientation of the specimen within the mould. To achieve the correct orientation, we first apply all the necessary transformations to the images, and then extract the volumes needed for mould design.

The first challenge concerns the direction along which the specimen has to be sectioned, following pathology protocols for renal cancer staging. To address it, we apply a 3D rotation to the images and create new slices that align with the preferred sectioning plane, which is defined by C_0 and the upper and lower pole ROIs.

The second challenge concerns the need to accurately place the specimen in the mould, even when it is covered in perinephric fat. We overcome this problem by defining reference landmarks that are expected to be exposed and identifiable in the specimen, and placing them at the base of the mould. These points act as anchors that ensure that the specimen is correctly positioned. The points are marked by carving 2 cm holes in the base of the mould that enable the pathologist to see and feel them, as shown in Figure 3. The two landmark points used for this purpose are the hilum and the tumour contact point.

Once the image has been rotated as desired, we extract the outline volume needed for the mould, and treat it as a set 3D structure with fixed orientation during the rest of the modelling process.

bioRxiv preprint doi: https://doi.org/10.1101/658831; this version posted June 3, 2019. The copyright holder for this preprint (which was not certified by peer review) is the author/funder, who has granted bioRxiv a license to display the preprint in perpetuity. It is made available under aCC-BY 4.0 International license.

Step 3: Mould optimisation and 3D printing

The volumetric matrix obtained after the re-orientation step is subsequently processed by applying a marching cubes algorithm. The resulting mesh is then reduced in its complexity by face reduction (target number of 5000), adaptive remeshing, three iterations of Laplacian smoothing, Taubin smoothing and several operations to ensure a closed mesh. Once the volume is smooth, it is carved off from a solid block-shaped base, and vertical slots are created to guide the knife during sectioning. The location of the inter-slot spaces is designed to match the exact location of the imaging slices. Finally, we carve holes with a diameter of 2cm at the contact and hilum landmark points. This entire process is automated [26].

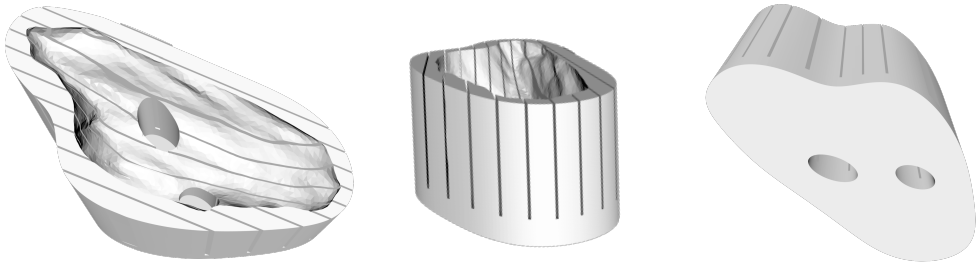

Fig 3. Optimised, patient-specific tumour mould. 3D rendering of the tumour mould viewed from three different angles showing the reference holes, sectioning slots and overall shape of the specimen.

Validation

The methodology was validated using a specimen from a 69-year-old man who underwent a laparoscopic radical nephrectomy. The tumour was a clear cell RCC (65 mm) with minimal tumour necrosis, invasion of the renal sinus fat and renal vein tributaries. Tumour stage was pT3a pNX, and Leibovich score of 6, meaning high risk of disease recurrence. MRI images were obtained 12 days before resection. The total volume of the lesion was 146 cm^3. Tumour, normal kidney and perinephric fat were delineated on a pre-surgical T1w MR image, as well as the hilum, renal pelvis, tumour contact point and kidney poles. The segmentations were checked by a radiologist with 15 years of experience in genitourinary imaging (ES). Images and landmarks were re-oriented using a MATLAB implementation of the method explained above, and a mould was automatically generated and 3D-printed [26]. The mould measured 8×18.6 cm and 3D printing took 18 hours. Reference points were marked with holes, as illustrated in Figure 3.

Habitats

Multiparametric MR images were co-registered and used to define spatial habitats inside the tumour using k-means clustering. In particular, we used T1w and T2w images, T1 map, K^{trans} from dynamic contrast enhanced (DCE) MRI as a measure of tumour vascular leakage, the diffusion coefficient and perfusion fraction from IVIM MRI imaging (f) as a measure of cellularity and tumour perfusion, and R2*, as a measure of oxygenation. We found three distinct habitats, as shown in Figure 4(e).

bioRxiv preprint doi: https://doi.org/10.1101/658831; this version posted June 3, 2019. The copyright holder for this preprint (which was not certified by peer review) is the author/funder, who has granted bioRxiv a license to display the preprint in perpetuity. It is made available under aCC-BY 4.0 International license.

Dissection and sectioning

The specimen was placed in the mould and sectioned 20 minutes after laparoscopic nephrectomy. The resection margin was inked for R-staging and all the perinephric fat was preserved. A slice with significant presence of all the habitats of the tumour, as well as being sufficiently separated from the hilum, was chosen for sectioning. The cut was made with a 12-inch CellPath Brain Knife.

Anatomical landmark validation

The slice provided a clean longitudinal cut of the kidney, including the renal pelvis and a cross section of the tumour, as illustrated in Figure 4(a). The tumour presented two hemorrhagic areas and a necrotic core.

The slice was photographed and reference tissues (tumour, kidney and renal pelvis) were manually contoured. The co-registration between MRI segmentations and tissue contours yielded Dice Similarity Coefficients (DSCs) [27] of 0.92 for the tumour, 0.75 for the renal pelvis and 0.76 for the kidney, as shown in Figure 4(c).

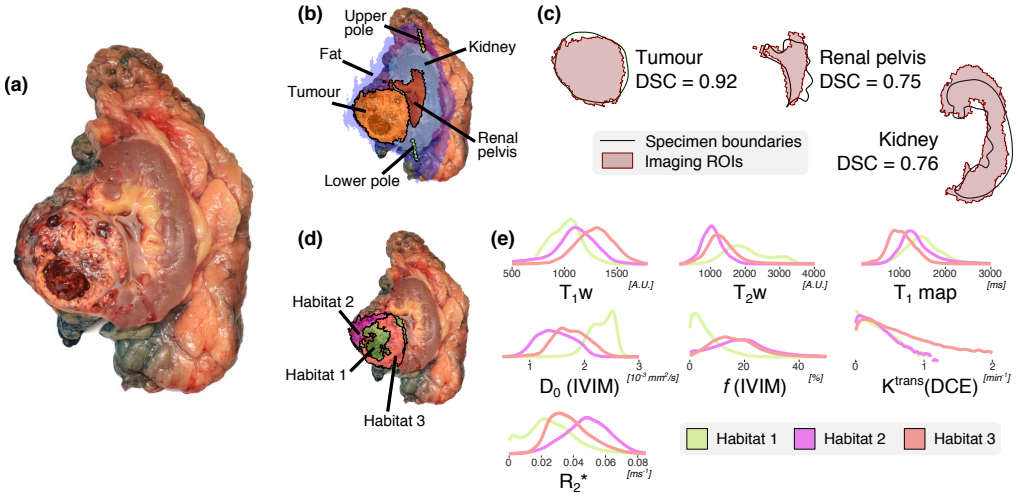

Fig 4. Image-guided sectioning. (a) Central slice of the resected specimen. (b) Overlay of the resected specimen and the anatomical structures delineated on the T1w scan. (c) Dice coefficients between the T1w-based segmentations and the observed tissue boundaries. (d) Overlay of the tumour habitats and the resected specimen. (e) Relative distributions of imaging parameters for the three tumour habitats.

Functional signal validation

All three habitats present with distinct distributions with respect to perfusion fraction f, K^{trans} and R2* maps, as shown in Figure 4(e). Habitat 1 was found to be poorly perfused and have a high diffusivity, T1w hypointensity and T2w hyperintensity. This habitat was found to overlap with the necrotic area found in the resected specimen, as shown in Figure 4(d).

Habitats 2 and 3 showed similar parametric distributions. Habitat 2 was adjacent to the kidney and showed the highest levels of K^{trans}. Habitat 3 showed the lowest diffusivity levels, as well as high R2*.

bioRxiv preprint doi: https://doi.org/10.1101/658831; this version posted June 3, 2019. The copyright holder for this preprint (which was not certified by peer review) is the author/funder, who has granted bioRxiv a license to display the preprint in perpetuity. It is made available under aCC-BY 4.0 International license.

Discussion

Capturing the full complexity of the disease is very challenging in cases like RCC, where tumours typically display a high degree of spatial heterogeneity both at the imaging and genomics level. In this paper we have presented a new methodology that overcomes one of the key problems in this area, namely the need to accurately match macroscopic habitats defined by imaging to specific tissue regions, without disrupting routine clinical practices. By integrating smoothly into clinical practice, our methodology has the potential to be widely applicable in clinical trials and therefore enable the creation of unprecedented datasets with matched imaging, histological and genomics data.

Mapping imaging and sectioning planes. Our approach was designed to address one of the limitations of previous 3D-printing-based co-registration methods, which assumed that tumours can be sectioned along the same plane that was used for MR imaging. This assumption generally interferes with pathology protocols. Commandeur et al. proposed a methodology to co-register histological planes to MRI slices for prostate cancer [28]. However, this co-registration has to be performed *a posteriori* and therefore the surgical biopsies would need to be obtained without image guidance, which might result in sub-optimal tumour sampling [10].

Instead, our approach uses a landmark system based on the definition of two reference points drawn by the radiologist on the MR scan (the upper and lower poles of the kidney). These points are then used to define the rotation to be applied to the images. We found that the rotation provided a longitudinal cut of the kidney, as expected.

Accurate co-registration in the presence of perinephric fat. The second challenge addressed by our approach is the presence of perinephric fat, which adds two complications to the tissue co-registration process: the difficulty in predicting the exact shape of the resected specimen, as the definition of optimal margins is controversial [29]; and the lack of an anatomical frame of reference to correctly position the specimen in the mould. Removing or trimming the fat may interfere with clinical practice, as it could compromise the surgical margins, which need to be evaluated for the presence of tumour cells [30]. A solution has been previously proposed for partial nephrectomy cases, using the inner parenchymal surface of the tumour as the base of the mould [25]. This method involved the surgeon inserting fiducial markers into the tumour during surgery, which interrupts the routine clinical pathway. In addition, partial nephrectomy is only recommended to treat small renal masses [31], so more advanced cases, which have typically poorer outcomes and are therefore of particular clinical relevance [32] would not be tractable with this approach.

Our methodology instead relies on a second set of key landmarks that can be used to orient the specimen even when there is a large component of fat. The landmarks used are the hilum, which can be identified by the presence of major blood vessels and the ureter emerging from the kidney, and a tumour or kidney area with thin or absent fat coverage. These reference points are placed at the base of the mould and marked with holes that allow the pathologist to confirm their correct positioning. This approach —combined with the first part of the re-orientation mechanism, which ensures that the sectioning is performed in the desired direction— resulted in an accurate co-registration between imaging and resected specimen. In particular, anatomical image segmentations were found to agree with the corresponding tissue outlines after mould-assisted sectioning, with DSCs ranging between 0.75 and 0.92. In addition, we observed that the tumour habitats identified from multiparametric MRI coincided with observable features of the tissue. For example, habitat 1 presented all the characteristics of necrotic

bioRxiv preprint doi: https://doi.org/10.1101/658831; this version posted June 3, 2019. The copyright holder for this preprint (which was not certified by peer review) is the author/funder, who has granted bioRxiv a license to display the preprint in perpetuity. It is made available under aCC-BY 4.0 International license.

tissue (poor perfusion, high diffusion, T1w hypointensity and T2w hyperintensity), and indeed coincided with the necrotic core of the tumour [33]. Similarly, habitat 3, which was closest to the normal kidney and therefore potentially could have better vascular access, was found to have high K^{trans}.

As expected, there was a thick layer of fat surrounding the kidney (see Figure 4), which made it impossible to see the kidney or identify its orientation by simple visual inspection. This would have been a challenge even in the standard clinical setting, and the pathologist found that the mould provided useful support and assistance aside from its research goals.

Limitations of the approach. Our approach shares some limitations with most other co-registration approaches. First of all, there is a time constraint between imaging and surgery. In this study imaging occurred 2 weeks before surgery, which could have resulted in anatomical changes and therefore an inadequate mould design. Shape-wise, additional uncertainty may arise from the segmentation of the structures on the MR images. Although several approaches for semi-automatic segmentation of kidney tumours exist [34–36], the preferred option is still manual contouring. Our methodology requires the additional delineation of perinephric fat, for which manual contouring, after discussion with the surgeon, is preferred. Although placing the point with the least fat coverage at the bottom of the mould helps reduce the uncertainty, intra-operative decisions may result in a different fat distribution. Having a single-sided mould (without an upper half) means that changes in the upper side of the specimen do not impact the accuracy, but any variations in the other half might. Finally, the methodology also requires validation in a larger patient cohort.

Impact and future work. The methodology we have presented here will be a core element of the WIRE renal cancer trial [37]. Future improvements to the mould design will include a cutting guide that directs the knife before it gets to the tumour, and an extension of the habitat definition to include radiomics features. By tightly integrating into the workflows of clinical trials, our methodology will enable the creation of large spatially-matched multiscale datasets including radiomics, genomics and histology data.

Material and Methods

Code

All the code necessary to reproduce these results, including volume orientation, 3D mould design, 3D printing, and habitat generation, can be found in doi:10.5281/zenodo.3066304.

Ethics

The method was designed as part of a physiological study currently being undertaken at the University of Cambridge with the aim of exploiting the integration of imaging and tissue based biomarkers to unravel tumor heterogeneity in renal cancer. The patient included in the present work received a laparoscopic radical nephrectomy. Informed consent was obtained for the Molecular Imaging and Spectroscopy with Stable Isotopes in Oncology and Neurology - substudy in renal cancer (MISSION) after prior approval by the East of England - Cambridge South ethics committee (REC: 15/EE/0378).

bioRxiv preprint doi: https://doi.org/10.1101/658831; this version posted June 3, 2019. The copyright holder for this preprint (which was not certified by peer review) is the author/funder, who has granted bioRxiv a license to display the preprint in perpetuity. It is made available under aCC-BY 4.0 International license.

MRI data acquisition

The 3D model of the tumour was designed based on a T1-weighted (T1w) MRI scan acquired using a Dixon imaging sequence (Table 1) acquired two weeks before surgery on a clinical 3T MRI (Discovery MR750, GE Healthcare, Waukesha, WI). Regions of interest (ROIs) were manually delineated by a radiologist on each slice of the MRI scan, using OsiriX (Version 10.0.0 [38]). The contours were drawn on coronal unenhanced T1w images using registered T2w and post-contrast T1w images to verify the accuracy of the ROIs. The segmentation was independently reviewed by a second radiologist. ROIs were exported from OsiriX to comma separated value files (.csv) encoding the coordinates of the edges of the ROI on each slice using the Export ROIs plugin (Version 1.9). The centroid of each ROI was calculated as the mean of all x, y and z coordinates of the voxels within it.

Table 1. MR Parameters

Sequence	TR [ms]	TE [ms]	Flip Angle [°]	Voxel size [mm^3]	Spacing [mm]	Comment
T1w Lava-Flex	3.7	1.1, 2.2	10	$1.6 \times 1.8 \times 4$	2	BH
T2w HyperCUBE	6000	96.8	90	$1.6 \times 1.8 \times 4$	2	RT
DWI (IVIM)	6666	78.9	90	$3.0 \times 3.0 \times 4$	2	RT b = 0, 10, 20, 30, 50, 100, 300, 500, 700, 900 s/mm^2
R2*mapping	110	2.3–36.2 (12 echoes)	30	$1.6 \times 1.8 \times 4$	4	multiple BH
T1 mapping Lava-Flex	3.7	1.1, 2.2	2, 3, 5, 8, 14	$2.0 \times 2.3 \times 4$	2	BH
DCE-MRI Lava-Flex	3.8	1.1, 2.2	18	$2.0 \times 2.3 \times 4$	2	multiple BH, 10 mins duration

TR: Repetition Time, TE: Echo Time, BH: Breath Hold, RT: Respiratory Triggering, DWI: Diffusion Weighted Imaging, IVIM: Intravoxel Incoherent Motion, DCE: Dynamic Contrast Enhanced. Voxel sizes give acquired resolutions.

Image pre-processing

Before generation of parameter maps, deformable motion correction was applied in MATLAB (Mathworks, Natick, MA) and utilizing ANTs/ITK [39]. In the case of DWI-MRI this was applied across acquisitions with differing b-values; in the case of DCE-MRI, this was applied across acquisition time-points and the associated T1 maps were transformed accordingly. Parameter maps were then generated using MATLAB in the case of DWI-IVIM, and using MIStar (Apollo Medical Imaging Technology, Melbourne, Australia) in the case of DCE-MRI, employing the Tofts model [40] and a model arterial input function. R2* maps were generated at source on the MR scanner using standard manufacturer software. All parameter map volumes were then aligned to the T1-weighted reference series used to prepare the mould. This was performed in two stages: first each parameter map volume was resampled into the space of the T1w reference series. Finally, and only if necessary, a rigid registration transform to more closely align the map with the reference image was determined manually using the software package ITK-SNAP; this transform was then applied to the parameter map volume.

bioRxiv preprint doi: https://doi.org/10.1101/658831; this version posted June 3, 2019. The copyright holder for this preprint (which was not certified by peer review) is the author/funder, who has granted bioRxiv a license to display the preprint in perpetuity. It is made available under aCC-BY 4.0 International license.

Mould orientation

The method proceeds as follows. First, the MR scan is re-sampled to achieve an isotropic resolution of $1 \times 1 \times 1$ mm^3 using nearest neighbour interpolation, as implemented in CERR [41]. Then, two three-dimensional rotations are applied. Several vectors connecting the structure centroids are defined to guide the re-orientation process, as follows:

$$v_{\mathrm{L}} = 0.5 \times (v_{\mathrm{hilum}} + v_{\mathrm{tumour\ contact}}), \tag{1}$$

$$v_{\mathrm{LC}} = v_{C_0} - v_{\mathrm{L}}, \tag{2}$$

$$v_{\mathrm{poles}} = v_{\mathrm{upper}} - v_{\mathrm{lower}}, \tag{3}$$

where v_i indicates the coordinates of the centroid of structure i, with v_{upper} representing the centroid of the upper pole, and v_{lower} the centroid of the lower pole. The first rotation aligns v_{LC} with the z axis. The second rotation aligns v_{poles} with the $x - z$ plane. Combined, the two rotations ensure that the orientation conditions are satisfied.

Before extracting and exporting the re-oriented volume for mould design, the surface is smoothed using 3D Gaussian filtering with a convolution kernel of size $9 \times 9 \times 9$ voxels and standard deviation of 3 voxels. Finally, the MR images are sliced along the $x - z$ plane with a spacing of 1 cm. These are used to build reference maps that will later guide the tissue sampling process; they also coincide with the location of the mould's slots.

3D printing

The model was sliced using Slic3r (Prusa Research, Czech) and printed with 0.2 mm layer height on a Prusa i3 MK3 printer loaded with RS PRO PLA filament (RS Components, UK).

Habitat clustering

In order to guide the process of tissue sampling, imaging maps were created for each tumour slice. The maps were obtained by combining multiparametric MR images and clustering them into several spatial clusters.

Along with the reference T1w images, additional sequences were acquired to define the phenotypic habitats. In particular, the images used for clustering were the T1w and T2w images, T1 map, K^{trans} from DCE MRI, the diffusion coefficient and perfusion fraction from IVIM MRI imaging (f), and R2*. Images were obtained on a 3T MR scanner, in coronal orientation with a slice thickness of 4 mm. Scans were corrected for motion artefacts and co-registered using rigid transformations. Additional details on the images, parameter maps, and methods can be found in Table 1 and the supplementary materials.

Habitats were obtained by applying k-means clustering on the set of co-registered images as well as the (x,y,z) coordinates corresponding to each voxel, to ensure spatial cohesion. The number of clusters was set to the maximum number that would allow taking three samples from each habitat. In practice, this translated into increasing the number of clusters until any of the habitats had an area smaller than approximately 3 cm^2.

Evaluation of spatial accuracy

The slice was placed on a flat, white surface and photographed. Tissue contours were drawn on the image, being completely blinded to the MRI segmentations. The resulting

bioRxiv preprint doi: https://doi.org/10.1101/658831; this version posted June 3, 2019. The copyright holder for this preprint (which was not certified by peer review) is the author/funder, who has granted bioRxiv a license to display the preprint in perpetuity. It is made available under aCC-BY 4.0 International license.

outline and the shape predicted after reorientation of the MR-segmentation were then overlayed and co-registered using manual rigid registration, maximising the overlap between the tumour contours. The accuracy of slice position recovery was assessed post-resection by comparing the DSC of MRI segmentations and the corresponding tissue contours. This coefficient is defined as:

$$DSC = \frac{2|X \cap Y|}{|X| + |Y|}$$

where the overlap of two binary masks X and Y (segmentations originating from different image sources) can be calcuated. The higher the DSC, the larger the overlap between the two binary masks.

Acknowledgments

The authors acknowledge the help of Gaspar Delso (GE Healthcare) and Dattesh Shanbhag (GE Global Research) for the use and ongoing support of their MR image motion-correction programming code. MCO acknowledges support from a Borysiewicz Fellowship from the University of Cambridge and Junior Research Fellowship from Trinity College, Cambridge. This work was supported by the Wellcome Trust (095962), Cancer Research UK (CRUK; C8742/A18097, C19212/A16628, C19212/A911376, C19212/A27150, C14303/A17197, C14303/A19274), the CRUK Engineering and Physical Sciences Research Council (EPSRC) Cancer Imaging Centre in Cambridge and Manchester (C197/A16465), the Mark Foundation Institute for Integrative Cancer Medicine at the University of Cambridge, Addenbrooke's Charitable Trust, the National Institute for Health Research (NIHR) Cambridge Biomedical Research Centre and Cambridge University Hospitals NHS Foundation Trust. Infrastructure for the Cambridge Urological Bio-repository was funded by the Cambridge Biomedical Research Campus and CRUK Cambridge Centre. Author ANP and the Human Research Tissue Bank are supported by the NIHR Cambridge Biomedical Research Centre.

References

1. Longo DL. Tumor Heterogeneity and Personalized Medicine. New England Journal of Medicine. 2012;366(10):956–957. doi:10.1056/NEJMe1200656.

2. Sankin A, Hakimi AA, Mikkilineni N, Ostrovnaya I, Silk MT, Liang Y, et al. The impact of genetic heterogeneity on biomarker development in kidney cancer assessed by multiregional sampling. Cancer medicine. 2014;3(6):1485–92. doi:10.1002/cam4.293.

3. Gerlinger M, Rowan AJ, Horswell S, Larkin J, Endesfelder D, Gronroos E, et al. Intratumor heterogeneity and branched evolution revealed by multiregion sequencing. New England journal of medicine. 2012;366(10):883–892.

4. Turajlic S, Xu H, Litchfield K, Rowan A, Chambers T, Lopez JI, et al. Tracking cancer evolution reveals constrained routes to metastases: TRACERx Renal. Cell. 2018;173(3):581–594.

5. Stewart GD, O'Mahony FC, Laird A, Eory L, Lubbock ALR, Mackay A, et al. Sunitinib Treatment Exacerbates Intratumoral Heterogeneity in Metastatic Renal Cancer. Clinical cancer research : an official journal of the American Association for Cancer Research. 2015;21(18):4212–23. doi:10.1158/1078-0432.CCR-15-0207.

bioRxiv preprint doi: https://doi.org/10.1101/658831; this version posted June 3, 2019. The copyright holder for this preprint (which was not certified by peer review) is the author/funder, who has granted bioRxiv a license to display the preprint in perpetuity. It is made available under aCC-BY 4.0 International license.

6. Okegawa T, Morimoto M, Nishizawa S, Kitazawa S, Honda K, Araki H, et al. Intratumor heterogeneity in primary kidney cancer revealed by metabolic profiling of multiple spatially separated samples within tumors. EBioMedicine. 2017;19:31–38.

7. Lubner MG, Stabo N, Abel EJ, del Rio AM, Pickhardt PJ. CT Textural Analysis of Large Primary Renal Cell Carcinomas: Pretreatment Tumor Heterogeneity Correlates With Histologic Findings and Clinical Outcomes. American Journal of Roentgenology. 2016;207(1):96–105. doi:10.2214/AJR.15.15451.

8. Yuan Q, Kapur P, Zhang Y, Xi Y, Carvo I, Signoretti S, et al. Intratumor Heterogeneity of Perfusion and Diffusion in Clear-Cell Renal Cell Carcinoma: Correlation With Tumor Cellularity. Clinical genitourinary cancer. 2016;14(6):e585–e594. doi:10.1016/j.clgc.2016.04.007.

9. Alessandrino F, Shinagare AB, Bossé D, Choueiri TK, Krajewski KM. Radiogenomics in renal cell carcinoma. Abdominal Radiology. 2018; p. 1–9. doi:10.1007/s00261-018-1624-y.

10. Soultati A, Stares M, Swanton C, Larkin J, Turajlic S. How should clinicians address intratumour heterogeneity in clear cell renal cell carcinoma? Current Opinion in Urology. 2015;25(5):358–366. doi:10.1097/MOU.0000000000000204.

11. Turajlic S, Xu H, Litchfield K, Rowan A, Horswell S, Chambers T, et al. Deterministic Evolutionary Trajectories Influence Primary Tumor Growth: TRACERx Renal. Cell. 2018;173(3):595–610.e11. doi:10.1016/j.cell.2018.03.043.

12. Mitchell TJ, Turajlic S, Rowan A, Nicol D, Farmery JHR, O'Brien T, et al. Timing the Landmark Events in the Evolution of Clear Cell Renal Cell Cancer: TRACERx Renal. Cell. 2018;173(3):611–623.e17. doi:10.1016/j.cell.2018.02.020.

13. Jhavar SG, Fisher C, Jackson A, Reinsberg SA, Dennis N, Falconer A, et al. Processing of radical prostatectomy specimens for correlation of data from histopathological, molecular biological, and radiological studies: a new whole organ technique. Journal of clinical pathology. 2005;58(5):504–8. doi:10.1136/jcp.2004.021808.

14. Madabhushi A, Feldman MD, Metaxas DN, Tomaszeweski J, Chute D. Automated detection of prostatic adenocarcinoma from high-resolution ex vivo MRI. IEEE Transactions on Medical Imaging. 2005;24(12):1611–1625. doi:10.1109/TMI.2005.859208.

15. Shah V, Pohida T, Turkbey B, Mani H, Merino M, Pinto PA, et al. A method for correlating in vivo prostate magnetic resonance imaging and histopathology using individualized magnetic resonance -based molds. Review of Scientific Instruments. 2009;80(10):104301. doi:10.1063/1.3242697.

16. Costa DN, Chatzinoff Y, Passoni NM, Kapur P, Roehrborn CG, Xi Y, et al. Improved Magnetic Resonance Imaging-Pathology Correlation With Imaging-Derived, 3D-Printed, Patient-Specific Whole-Mount Molds of the Prostate. Investigative Radiology. 2017;52(9):507–513. doi:10.1097/RLI.0000000000000372.

17. Ebbing J, Jäderling F, Collins JW, Akre O, Carlsson S, Höijer J, et al. Comparison of 3D printed prostate models with standard radiological information to aid understanding of the precise location of prostate cancer: A construct validation study. PLOS ONE. 2018;13(6):e0199477. doi:10.1371/journal.pone.0199477.

bioRxiv preprint doi: https://doi.org/10.1101/658831; this version posted June 3, 2019. The copyright holder for this preprint (which was not certified by peer review) is the author/funder, who has granted bioRxiv a license to display the preprint in perpetuity. It is made available under aCC-BY 4.0 International license.

18. Weigelt B, Vargas H, Selenica P, Geyera P, Mazaheri Y, Blecua P, et al. Radiogenomics analysis of intra-tumor heterogeneity in a patient with high-grade serous ovarian cancer. JCO Precision Oncology. 2019 (in press);.

19. Sun Z, Liu D. A systematic review of clinical value of three-dimensional printing in renal disease. Quantitative imaging in medicine and surgery. 2018;8(3):311–325. doi:10.21037/qims.2018.03.09.

20. Warren AY, Griffiths D, Fleming S. Dataset for histopathological reporting of adult renal parenchyma neoplasms; 2017. Available from: `https://www.rcpath.org/uploads/assets/uploaded/22496153-93f9-4004-87021102dc32ac6c.pdf`.

21. Trpkov K, Grignon DJ, Bonsib SM, Amin MB, Billis A, Lopez-Beltran A, et al. Handling and Staging of Renal Cell Carcinoma. The American Journal of Surgical Pathology. 2013;37(10):1505–1517. doi:10.1097/PAS.0b013e31829a85d0.

22. King S DM. Kidney renal parenchymal tumour. In: Anatomical Pathology Macroscopic Cut-up Manual. Surry Hills NSW: Royal College of Pathologists of Australasia; 2017.Available from: `https://www.rcpa.edu.au/Library/Practising-Pathology/Macroscopic-Cut-Up/Specimen/Genitourinary/Kidney/Kidney-renal-parenchyma`.

23. Krabbe LM, Bagrodia A, Margulis V, Wood CG. Surgical management of renal cell carcinoma. Seminars in interventional radiology. 2014;31(1):27–32. doi:10.1055/s-0033-1363840.

24. Disselhorst JA, Krueger MA, Ud-Dean SM, Bezrukov I, Jarboui MA, Trautwein C, et al. Linking imaging to omics utilizing image-guided tissue extraction. Proceedings of the National Academy of Sciences. 2018;115(13):E2980–E2987.

25. Dwivedi DK, Chatzinoff Y, Zhang Y, Yuan Q, Fulkerson M, Chopra R, et al. Development of a Patient-specific Tumor Mold Using Magnetic Resonance Imaging and 3-Dimensional Printing Technology for Targeted Tissue Procurement and Radiomics Analysis of Renal Masses. Urology. 2018;112:209–214. doi:10.1016/j.urology.2017.08.056.

26. Cutter: 3D-printed moulds for image-guided tumour biopsies; 2019. Available from: `https://zenodo.org/record/3066305`.

27. Dice LR. Measures of the amount of ecologic association between species. Ecology. 1945;26(3):297–302.

28. Commandeur F, Acosta O, Simon A, Mathieu R, Fautrel A, Gnep K, et al. Prostate whole-mount histology reconstruction and registration to MRI for correlating in-vivo observations with biological findings. In: 2015 37th Annual International Conference of the IEEE Engineering in Medicine and Biology Society (EMBC). IEEE; 2015. p. 2399–2402. Available from: `http://ieeexplore.ieee.org/document/7318877/`.

29. Picken MM, Wang L, Gupta GN. Positive Surgical Margins in Renal Cell Carcinoma. American Journal of Clinical Pathology. 2015;143(5):620–622. doi:10.1309/AJCP9KVHJRXF6DBZ.

30. Association of Directors of Anatomic and Surgical Pathology. Recommendations for the Reporting of Surgically Resected Specimens of Renal Cell Carcinoma:. American Journal of Clinical Pathology. 2009;131(5):623–630. doi:10.1309/AJCP84ESGXKXYNRA.

bioRxiv preprint doi: https://doi.org/10.1101/658831; this version posted June 3, 2019. The copyright holder for this preprint (which was not certified by peer review) is the author/funder, who has granted bioRxiv a license to display the preprint in perpetuity. It is made available under aCC-BY 4.0 International license.

31. Cozar JM, Tallada M. Open partial nephrectomy in renal cancer: a feasible gold standard technique in all hospitals. Advances in urology. 2008;2008:916463. doi:10.1155/2008/916463.

32. Kutikov A, Egleston BL, Wong YN, Uzzo RG. Evaluating Overall Survival and Competing Risks of Death in Patients With Localized Renal Cell Carcinoma Using a Comprehensive Nomogram. Journal of Clinical Oncology. 2010;28(2):311–317. doi:10.1200/JCO.2009.22.4816.

33. Pedrosa I, Sun MR, Spencer M, Genega EM, Olumi AF, Dewolf WC, et al. MR Imaging of Renal Masses: Correlation with Findings at Surgery and Pathologic Analysis. RadioGraphics. 2008;28(4):985–1003. doi:10.1148/rg.284065018.

34. Skalski A, Jakubowski J, Drewniak T. Kidney tumor segmentation and detection on Computed Tomography data. In: 2016 IEEE International Conference on Imaging Systems and Techniques (IST). IEEE; 2016. p. 238–242. Available from: `http://ieeexplore.ieee.org/document/7738230/`.

35. Zhou B, Chen L. Atlas-based semi-automatic kidney tumor detection and segmentation in CT images. In: 2016 9th International Congress on Image and Signal Processing, BioMedical Engineering and Informatics (CISP-BMEI). IEEE; 2016. p. 1397–1401. Available from: `http://ieeexplore.ieee.org/document/7852935/`.

36. Bücking TM, Hill ER, Robertson JL, Maneas E, Plumb AA, Nikitichev DI. From medical imaging data to 3D printed anatomical models. PLOS ONE. 2017;12(5):e0178540. doi:10.1371/journal.pone.0178540.

37. WIRE - Novel Treatments in Renal Cell Cancer (WIRE); 2019. Available from: `https://clinicaltrials.gov/ct2/show/NCT03741426`.

38. Rosset A, Spadola L, Ratib O. OsiriX: An Open-Source Software for Navigating in Multidimensional DICOM Images. Journal of Digital Imaging. 2004;17(3):205–216. doi:10.1007/s10278-004-1014-6.

39. Avants BB, Tustison NJ, Stauffer M, Song G, Wu B, Gee JC. The Insight ToolKit image registration framework. Frontiers in neuroinformatics. 2014;8:44. doi:10.3389/fninf.2014.00044.

40. Tofts PS, Brix G, Buckley DL, Evelhoch JL, Henderson E, Knopp MV, et al. Estimating kinetic parameters from dynamic contrast-enhanced T(1)-weighted MRI of a diffusable tracer: standardized quantities and symbols. Journal of magnetic resonance imaging : JMRI. 1999;10(3):223–32.

41. Deasy JO, Blanco AI, Clark VH. CERR: A computational environment for radiotherapy research. Medical Physics. 2003;30(5):979–985. doi:10.1118/1.1568978.